Journal of Materials Research and Technology 28 (2024) 1514–1522

Contents lists available at ScienceDirect

Journal of Materials Research and Technology

journal homepage: www.elsevier.com/locate/jmrt

A better understanding of hydrogen trapping and diffusion in aluminized press-hardenable steels

M. Krid [a,b], M. Mandy [b], T. Sturel [c], R. Grigorieva [c], P. Drillet [c], P.J. Jacques [a,*]

[a] UCLouvain, Institute of Mechanics, Materials and Civil Engineering, IMAP, 1348, Louvain-la-Neuve, Belgium
[b] CRM Group, 4000, Liège, Belgium
[c] ArcelorMittal Global R&D, 57283, Maizières-lès-Metz Cedex, France

ARTICLE INFO

Handling editor:P Rios

Keywords:
Aluminzed steels
Deuterium
Diffusion
Coatings
TDA

ABSTRACT

Press hardenable steels (PHS) coated with Al–Si alloy are widely used in the automotive industry owing to their good mechanical properties (Yield Strength >1200 MPa and Tensile Strength >1500 MPa). The presence of Al–Si coating prevents oxidation and decarburization of steel during austenitization. However, aluminized PHS are sensitive to hydrogen absorption during austenitization, while Al–Si coating prevents hydrogen degassing from the specimen at room temperature so that diffusible hydrogen could lead to hydrogen embrittlement in specific conditions.

In this study, H trapping in aluminized steels was critically assessed using deuterium sources instead of hydrogen sources during austenitization and thermal desorption analysis (TDA). 22MnB5 steel coated with Al and Al–Si alloys were studied. D is mainly trapped in the dislocations strain field in the steel substrate of aluminized steels and it is responsible for the three main D_2 desorption peaks in Al and Al–Si coated steels. Multiple peaks observed on D_2 desorption profiles of Al and Al–Si coated steels are explained by the preferential desorption path of D depending on the sample temperature.

1. Introduction

Over the last decades, growing demand for fuel efficient vehicles has led the automotive industry to create lighter cars with an improvement of safety and crashworthiness. In this context, press hardened steels (PHS) are more and more used in the structural components, due to their high strength to mass ratio [1,2]. They are produced by hot stamping process which combines microstructural optimization and shaping of complex geometries of steels without any residual deformation or spring-back [2]. During this process, cold-rolled steels are classically austenitized at 900 °C for 5–10 min and subsequently transferred into a cold die to perform simultaneously forming and quenching bringing a martensitic microstructure [3]. 22MnB5-related steels are the most common steel grades used for hot stamping process and present an ultimate tensile strength of approximatively 1500 MPa and a yield strength of approximatively 1200 MPa after press hardening [4].

Austenitization is commonly carried out in air without any control, particularly of the present humidity characterized by the dew point, causing elevated temperature oxidation and decarburization of the steel surface. Therefore, PHS are usually precoated with an Al–Si coating by hot dip aluminizing to provide a high temperature and a life service corrosion protection. However, previous studies have demonstrated that aluminized PHS are more sensitive to H absorption during austenitization compared to uncoated PHS [5,6]. Indeed, high temperature decomposition of water vapor by Al–Si coating is responsible for H pick-up during austenitization. H adsorbed on the surface diffuses through the coating to reach the steel substrate due to his high diffusivity at elevated temperature in aluminium and iron-aluminium intermetallic phases compared to austenite [7–12]. After quenching, Al–Si coating prevents H degassing from the specimen at room temperature, which remains mostly trapped in the martensite matrix of the steel substrate [5].

Hydrogen in metals is distributed among interstitials sites in the crystal lattice and microstructural defects such as grain boundaries, dislocations and vacancies. These sites are qualified as reversible or irreversible traps depending on the activation energy that must be supplied for H to be released [13] and tuning the hydrogen embrittlement phenomenon [14]. Hydrogen embrittlement (HE) is a significant concern in the development of ultra-high strength steel for the automotive industry. Indeed, 22MnB5 steels present a low resistance to HE

* Corresponding author.
E-mail address: pascal.jacques@uclouvain.be (P.J. Jacques).

https://doi.org/10.1016/j.jmrt.2023.11.214
Received 14 September 2023; Received in revised form 20 November 2023; Accepted 22 November 2023
Available online 27 November 2023

due to the high mobility of hydrogen in the BCC lattice causing hydrogen delayed fracture under applied stress [15]. This phenomenon is especially pronounced in high strength steels even at concentrations of H below 1 wt.ppm [16,17].

Several techniques such as electrochemical permeation, gas permeation and inert gas fusion allow to quantify H present in steels and to determine its mobility in the lattice. Among those techniques, thermal desorption analysis (TDA) enables to calculate both the concentration of diffusible H and its diffusivity, while providing information about its distribution through various microstructural defects in metals [18].

Several authors reported TDA measurements of hydrogen desorption profiles of aluminized PHS. For instance, *Cho* et al. [19] showed that H_2 desorption profiles of aluminized 35MnB5 steel after hot stamping present one desorption peak at 200 °C and a second one at 500 °C [19]. Using Kissinger theory, they assigned the first H_2 desorption rate peak to H trapping in the strain field of dislocations in the martensitic microstructure of the steel substrate. Furthermore, they stated that the second H_2 desorption rate peak is related to H trapped in the core of dislocations in the martensitic microstructure of the steel substrate in both uncoated and aluminized PHS. However, this second peak is difficult to distinguish from the background noise on thermal desorption profiles of uncoated PHS. *Georges* et al. [6] demonstrated through degassing experiments at room temperature that the second H_2 desorption rate peak is related to H trapped in the aluminized PHS.

In order to confirm whether H remains trapped in the Al–Si coating or in the steel substrate after hot stamping process, *Georges* et al. [5] and *Jo* et al. [20] performed mechanical removal of the coating on aluminized PHS before TDA. They measured either a lower or an equal concentration of H after grinding, and concluded that H is mostly trapped inside the steel substrate and not in the Al–Si coating. Nevertheless, these measurements were carried out on a reduced number of samples, without considering the possible risks of contaminations linked to atmospheric sources of H, such as the presence of water vapor. Besides, the Al–Si coating represents a low percentage of the total mass of the aluminized steel, and small changes of H concentration evaluated by TDA for coating stripped specimen compared to aluminized specimen would lead to large differences in the calculated H concentrations in the coating.

Finally, several authors observed a shift of H_2 desorption peak for aluminized PHS compared to uncoated PHS [5,19–22] and concluded that the Al–Si coating acts as a barrier to H diffusion. Indeed, *Kuhlmann* et al. [22] calculated an effective H diffusion coefficient of $3.8\ 10^{-13}\ m^2.s^{-1}$ at 25 °C for aluminized PHS, which is two orders of magnitude lower than 22MnB5 uncoated PHS. However, they could not assign which phases of the Al–Si coating are responsible for this barrier effect.

The aim of the present study is to critically assess the potential H trapping sites in aluminized PHS after hot stamping process. Quite uniquely, deuterium sources are used instead of hydrogen sources during austenitization to avoid any atmospheric contamination, which could compromise further quantification during TDA measurements. For this purpose, a combined approach of degassing experiment at room temperature and calculation of hydrogen detrapping activation energy in aluminized steels after mechanical removal of the coating will be used to correctly assign hydrogen trapping sites on the basis of the TDA profiles of aluminized steels.

2. Materials and experimental methods

2.1. Materials and heat treatment

Industrial Al–Si and Al coated samples were considered in this study. They are produced from cold rolled 22MnB5 steel sheets which were at first annealed at 800 °C and then dipped in molten baths at 675 °C containing either 88 wt % Al, 9 wt % Si, 3 wt % Fe or 97 wt % Al, 3 wt % Fe, respectively. The final thickness of aluminized PHS was 1.20 mm. The chemical composition of the steel substrate obtained by optical emission spectroscopy (OES) is given in Table 1, while its initial microstructure was constituted of ferrite-pearlite.

Heat treatments were performed in a muffle furnace pre-heated at 920 °C on 100-by-200 mm^2 steel sheets degreased with ethanol. The atmosphere in this muffle furnace was controlled by injecting controlled amounts of $N_{2\ (g)}$ and $D_2O_{(g)}$. N_2 atmosphere was used instead of air to maximize D uptake. Humidity was measured by a hygrometer and characterized by the dew point. The latter was set at + 12.5 °C by adjusting the dry gas ($N_{2\ (g)}$) and wet gas ($N_{2\ (g)} + D_2O_{(g)}$) flows, which corresponds to an amount of 1.2 % mol of $D_2O_{(g)}$ in the atmosphere. This wet gas resulted from bubbling $N_{2\ (g)}$ dry gas into liquid $D_2O_{(l)}$. A thermocouple was spot-welded on the samples to record the temperature evolution during heat treatment. Hot stamping was simulated by austenitizing samples at 900 °C for 10 min followed by quenching in water at 85 °C to achieve a fully martensitic microstructure. Other heat treatments were performed at 900 °C during 0 and 30 min to evaluate the impact of dwell time on D uptake and trapping. After heat treatments, aluminized sheets were cut into samples of 20 by 30 mm^2 and then stored in liquid nitrogen to prevent from D degassing.

2.2. Thermal desorption analysis

Prior to measurements, samples were degreased with acetone in an ultrasonic bath. A thermocouple was then spot-welded. During TDA, samples were heated at a constant rate owing to an IR furnace, activating detrapping and diffusion of H or D. A dry gas ($N_{2(g)}$) sweeps the samples and carries $D_{2(g)}$ or $H_{2(g)}$ to a selective quadrupole mass spectrometer. This device allowed the quantification of $D_{2(g)}$or $H_{2(g)}$ owing to calibration twice a day with two certified gases containing 50 ppm of $H_{2(g)}$ or $D_{2(g)}$ mixed with $N_{2(g)}$.

The low abundance of D in the atmosphere ensured that $D_{2(g)}$ desorbed during TDA originates only from D introduced in the specimen during charging procedure. However, atmospheric sources of H present during samples preparation or austenitization also lead to desorption of $H_{2\ (g)}$ during TDA, and the presence of both isotopes can lead to $HD_{(g)}$ recombination [23]. In order to consider this isotopic exchange reaction, both $D_{2(g)}$ and $HD_{(g)}$ flux were measured by the mass spectrometer and used to calculated the total concentration of D in the specimen, expressed in 10^{-6} mol g^{-1}. This unit corresponds to the number of moles of D in both $D_{2(g)}$ and $HD_{(g)}$ desorbed per gram of steel. However, there exists no certified gas for the HD calibration. As a result, the HD calibration factor was calculated as the mean value of the $D_{2(g)}$ and the $H_{2(g)}$ calibration factors.

A heating rate of 20 °C min^{-1} was used during the first set of TDA measurements. The setpoint temperature was 800 °C for D desorption. In order to calculate a detrapping activation energy for D desorption, a second set of TDA measurements was carried out by varying heating rates from 5 °C min^{-1} to 20 °C min^{-1}.

2.3. Mechanical removal of the coating

In order to assess D trapping in aluminized PHS, mechanical removal of the coating was performed for some samples prior to TDA. The impact of grinding on the concentration of D was determined by comparing two samples, a coated one and a coating stripped one, initially located next to each other in the middle of the steel sheet during the charging heat treatment, the latter precaution enabling to optimize homogeneity of hydrogen distribution in both samples. Grinding was carried out very softly with steps of 3 μm to avoid any heating. Cooling medium was also used.

Table 1
OES analysis of 22MnB5 steel substrate (mass %).

C	Si	Mn	P	S	Cr
0.245	0.267	1.24	<0.05	<0.05	0.182

2.4. Microstructure characterization

Prior to the microstructural analysis, cross sections of specimens were mechanically ground and polished. A final polishing step was performed using colloidal silica suspension (particle size of 0.04 μm). Polished specimens were etched with a 2 % nital solution during 10 s–15 s to reveal the steel microstructure.

Scanning Electron Microscopy (SEM) observations were conducted to determine the microstructure of coated steels after austenitization. The accelerating voltage was set at 15 kV for secondary or backscattered electrons imaging. Energy Dispersive X-ray Spectroscopy (EDX) was used to quantify the chemical composition of the phases of both coatings. The working distance was set at 6 mm and the aperture size was set at 60 μm for BSE imaging. The working distance and aperture size were set at 6 mm and 120 μm for EDS analysis.

3. Results and discussion

3.1. Microstructure of aluminized PHS after austenitization

The microstructure of the Al–Si coated 22MnB5 steel heat treated at 900 °C for 10 min followed by water quenching consist of layers of Fe–Al–Si intermetallic (Fig. 1A point 1), τ_1, in intermetallics Fe_2Al_5 (Fig. 1A points 2 and 3) together with a martensitic steel substrate. This microstructure is very close to the one found in previous studies for the same coating after austenitization treatment at 900 °C during 10 min [24,25]. The richer Si phase is dispersed as islands near the coating surface (Fig. 1A point 1), and has already been identified as both FeAl + $Fe_3Al_2Si_3$ (τ_1) [25–28]. An interdiffusion layer (Fig. 1A point 4), 10 μ m in thickness, identified as α-Fe (Al,Si) can be observed at the interface with the steel substrate. Its evolution is driven by solid state diffusion of Al from the coating to the steel substrate during heating [26].

After heat-treatment, the Al coating presents a simpler microstructure with three layers: one richer in Fe in the vicinity of the steel substrate (Fig. 1B points 2 and 3), and the other ones richer in Al close to the coating surface (Fig. 1B point 1). The EDS analysis (Table 2) identified the upper part of the coating as Fe_2Al_5 (Fig. 1 b point 1) and FeAl (Fig. 1 b point 2). Similar to the Al–Si coating, an interdiffusion layer (Fig. 1 b point 3) identified as α-Fe (Al) of 15 μ m thickness delimits the coating from the steel substrate.

Both coatings show cracks that extend from the surface to the interdiffusion layer. These cracks most probably result from several factors: thermal stresses during quenching, differences in the thermal expansion coefficient between the intermetallic compounds and the steel substrate, and the low toughness of the Al-rich intermetallic compounds constituting the coating matrix after austenitization [29].

Table 2
SEM-EDS point analysis (at. %) and the corresponding phases composition for Al and Al–Si coated steels heat treated at 900 °C during 10 min and followed by quenching.

		Fe	Al	C	O	Si	Phases
22MnB5 + Al	Point 1	35	56	7	1	0	Fe_2Al_5
	Point 2	59	31	7	2	0	FeAl
	Point 3	72	17	8	3	0	α-Fe (Al)
22 MnB5 + Al–Si	Point 1	50	35	/	3	12	FeAl(Si)
	Point 2	38	57	/	3	2	Fe_2Al_5
	Point 3	32	50	14	3	2	Fe_2Al_5
	Point 4	64	13	12	3	7	α-Fe (Al,Si)

3.2. TDA of bare steels and aluminized steels

The D_2 desorption curves of Al–Si coated steels (Fig. 2) clearly exhibit two distinct peaks centred at 175 °C and 400 °C, respectively; while the D_2 desorption profile of Al coated steels exhibits three peaks centred at 150 °C, 280 °C and 500 °C, respectively. On the other hand, desorption profiles of bare steel present only one peak centred at 150 °C. These observations indicate that D desorption process through coated steels and bare steels are significantly different. The concentrations of D evaluated by TDA of aluminized steels (Fig. 3) are significantly higher than the one in bare steel. It can thus be argued that the Al and Al–Si coatings increase D pick-up during austenitization of aluminized steels.

3.3. Effect of grinding of aluminized steels

Figs. 4 and 5 show the desorption profiles of Al and Al–Si coated steels before and after mechanical removal of the coating. In the case of aluminized steels, the D_2 desorption peaks at 200°C–250 °C and 400°C-

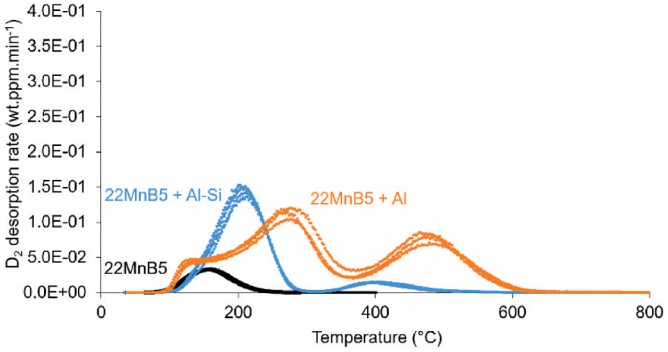

Fig. 2. D_2 desorption curves of aluminized steels compared to 22MnB5 bare steel after austenitization at 900 °C for 10 min and water quenching.

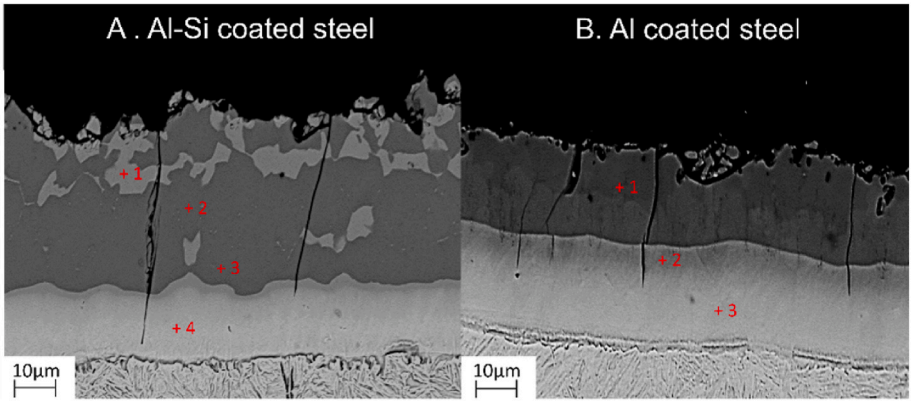

Fig. 1. SEM backscatter micrographs of (A) Al–Si coated 22MnB5 steel austenitized at 900 °C for 10 min and water quenched in water at 85 °C; (B) Al coated 22MnB5 steel austenitized at 900 °C for 10 min and water quenched in water at 85 °C.

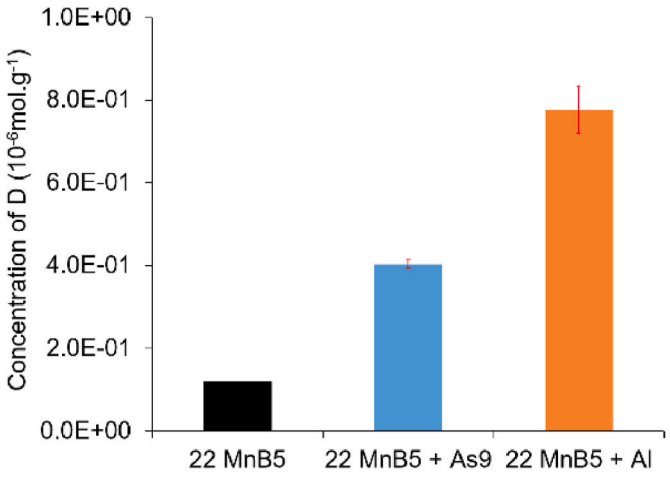

Fig. 3. Concentration of D measured in aluminized and bare steels heat treated at 900 °C during 10 min followed by quenching in water at 85 °C. Standard deviation are represented by red bars. (For interpretation of the references to colour in this figure legend, the reader is referred to the Web version of this article.)

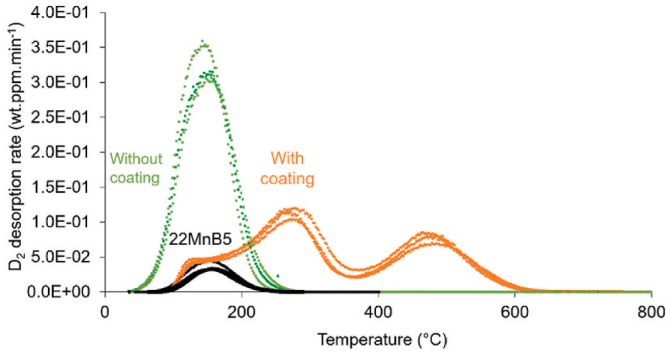

Fig. 4. D_2 desorption curves of Al coated steel heat treated at 900 °C for 10 min before and after grinding compared to bare steel austenitized in the same condition.

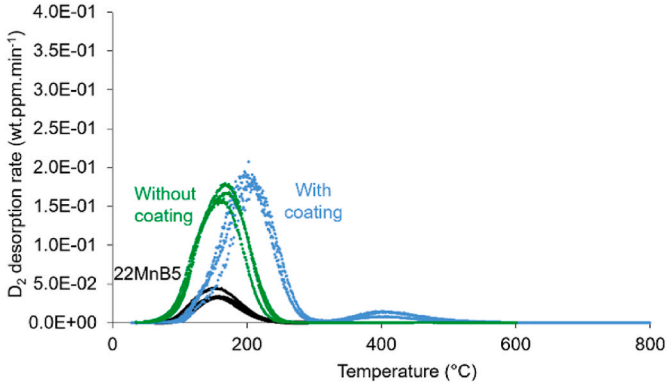

Fig. 5. D_2 desorption curves of Al–Si coated steel heat treated at 900 °C for 10 min before and after grinding compared to bare steel austenitized in the same condition.

500°Care related to the presence of the coating. After mechanical removal of both coatings, the only remaining desorption peak is centred at the same temperature than in the case of the bare steel. Therefore, a main question about the location of D and the origin of high temperature D_2 desorption peaks in aluminized steels is raised: Is a part of D trapped in the coating or not? Indeed, different desorption peaks in the coating suggest different traps, while after grinding only one peak remains, attributed to one specific deuterium trap.

In order to determine whether the high temperature D_2 desorption peaks are related to the trapping of deuterium in the coating or not, concentrations of deuterium in aluminized steel before and after grinding are compared in Fig. 6. Assuming a homogeneous distribution of deuterium through the steel substrate and the coating, grinding of aluminized steels should not cause any reduction or any increase of concentration of deuterium evaluated by TDA. In the case of Al–Si coated steels, the concentration of deuterium measured for samples after grinding is 0.05 10^{-6} mol. g^{-1}, lower than before grinding. This indicates that some of the deuterium could be trapped in the Al–Si coating. However, standard deviation related to this concentration is of the same order of magnitude as the estimated concentration of deuterium. In the case of Al coated steels, grinding leads to a small increase of the concentration of deuterium evaluated by TDA, which means that deuterium is mostly trapped in the steel substrate. The concentration of D, C_D, in the removed layer is calculated by subtracting the concentration of D in aluminized steels to the one in specimen after coating removal (Eq. (1)). If we define two samples (a coated one and a coating stripped one), in which the deuterium concentrations are measured (respectively, C_1 and C_2) (expressed in 10^{-6} mol g^{-1}), the estimated D concentration in the removed layer C_D is expressed as:

$$C_D = \frac{c_1 w_1 - c_2 w_2}{w_1 - w_2} = \frac{c_1 w_1 - c_2 0,01X\, w_1}{w_1 - w_1 0,01X} = \frac{w_1 (c_1 - 0,01X c_2)}{w_1\,(1 - 0,01X1^2)} = \frac{(c_1 - 0,01X c_2)}{(1 - 0,01X)} \quad \text{(Eq. 1)}$$

Where, w_1 and w_2 are the masses before and after grinding of a coated stripped specimen in g and X corresponds to the remaining mass after grinding expressed in %. C_D calculated in the removed layer to the third bar for each material in Fig. 6.

The concentration of D in the removed layer is significantly lower than in the steel substrate for Al coated steels, and the opposite is observed for Al–Si coated steels. The calculated standard deviation is extremely large and could result from a combination of two factors: a small difference between the concentration of D measured between the coated steel and the grinded steel and the fact that small changes of concentration of D between coating stripped sample and aluminized samples will lead to large differences in the concentrations of D calculated in the removed layer.

These results revealed that the majority of D is trapped in the steel

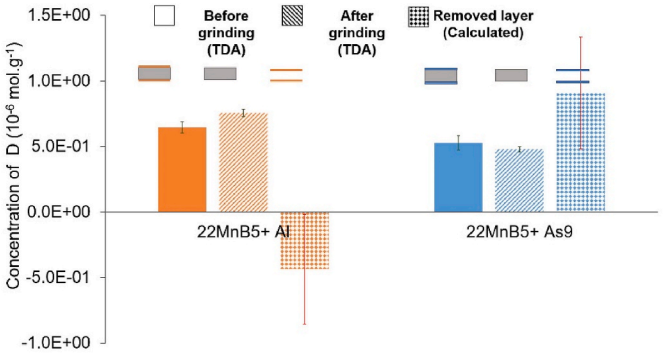

Fig. 6. Concentration of D in Al–Si and Al coated steel heat treated at 900 °C during 10 min (N_2 + D_2O) before grinding (full bars) and after grinding (hatched bars) compared to the concentration of D calculated in the removed layer (bars with tile pattern).The standard deviation are presented with black bars for the concentration of D measured by TDA in aluminized steels and coating stripped steels, and they are presented with red bars for the concentration of D calculated in the removed layer. (For interpretation of the references to colour in this figure legend, the reader is referred to the Web version of this article.)

substrate in aluminized steels and should be responsible for all D_2 desorption peaks in Al coated steel and at least the D_2 desorption peak centred at 200 °C in Al–Si coated steel. High temperature D_2 desorption peak in Al–Si coated steels could be caused by D trapping in the coating or in the steel substrate.

3.4. Evaluation of detrapping activation energy

Several studies considered the determination of the H detrapping activation energy using the Kissinger theory for a first order desorption kinetic (Eq.2) [30,31]. In practice, it consists in carrying out TDA of samples at different heating rates and measuring the resulted shift of H_2 or D_2 maximum desorption rate temperature:

$$\frac{d \ln \frac{\Phi}{T_{peak}^2}}{d \frac{1}{T_{peak}}} = -\frac{E_d}{R} \quad \text{(Eq.2)}$$

Where, T_{peak} is the temperature (K) for which H release rate is maximum, E_d is the detrapping energy required for H or D desorption from a specific trap corresponding with T_{peak} in kJ.mol^{-1}, Φ corresponds to the heating rate in K min^{-1} and R the ideal gas constant 8.314J/mol K. By increasing the heating rate, D_2 desorption peaks of Al and Al–Si coated steels are shifted to higher temperatures as shown in Figs. 7 and 8. The maximum desorption flux intensity was also reduced for higher heating rates, which is attributed to a longer test duration.

By applying this procedure, we assume that each desorption peak is caused by a specific trap releasing D. Activation energies are extracted from the slope of the line of Choo-Lee plots in Fig. 9 (coated steels) and Fig. 10 (after mechanical removal of the coating) using Eq.2 and reported in Table 3. Detrapping activation energies calculated for the first desorption peaks in Al and Al–Si coated steels and the only desorption peak on desorption profile of coating stripped samples are ranging from 27 kJ mol^{-1} to 32 kJ mol^{-1}. According to the literature, this should correspond to D located in dislocation stress fields in martensitic steels [18,19]. These observations are in good agreement with those made by previous studies, who worked on the H embrittlement of 22MnB5 steels [18,21]. They have demonstrated by means of TDA and electro-chemical permeation techniques (EP) that H in hot stamped 22MnB5 steel is located in reversible traps and more precisely in the dislocation stress fields in the martensitic phase.

The activation energies calculated for the second and third desorption peaks in Al coated steel and the third desorption peak in Al–Si coated steel are higher than 50 kJ mol^{-1}. These peaks should correspond to D irreversibly trapped in the material, for example, in a dislocation core or in high angle boundaries.

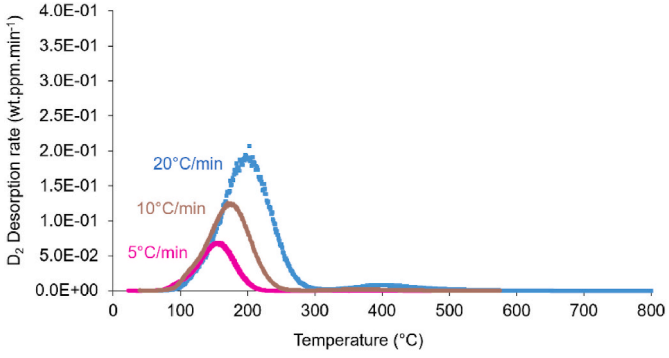

Fig. 7. Evolution of D_2 desorption profiles of Al–Si coated steel heat treated at 900 °C during 10 min as a function of the heating rate. Three heating rates were used 5 °C.min^{-1} (pink), 10 °C.min^{-1} (brawn) and 20 °C.min^{-1} (blue). (For interpretation of the references to colour in this figure legend, the reader is referred to the Web version of this article.)

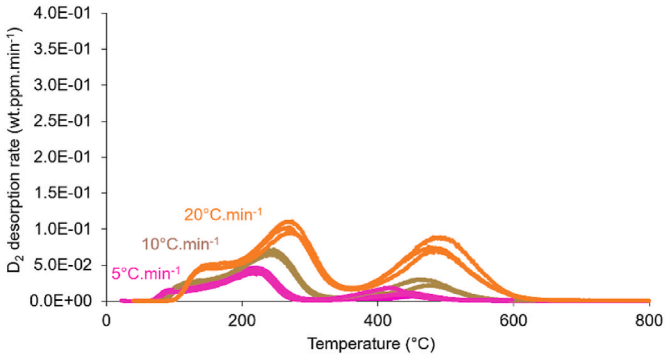

Fig. 8. Evolution of D_2 desorption profiles of Al coated steel heat treated at 900 °C during 10 min as a function of the heating rate. Three heating rates were used 5 °C.min^{-1} (pink), 10 °C.min^{-1} (brawn) and 20 °C.min^{-1} (orange). (For interpretation of the references to colour in this figure legend, the reader is referred to the Web version of this article.)

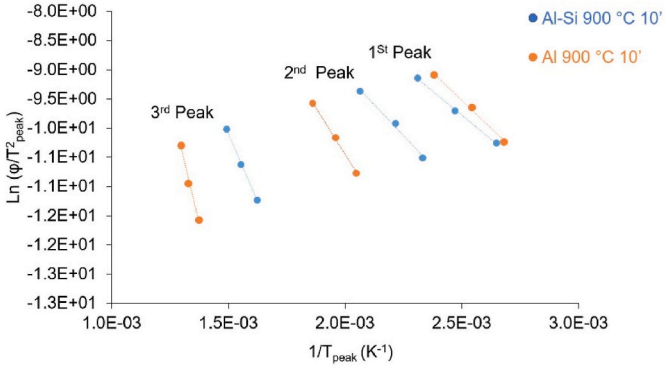

Fig. 9. Choo-Lee plot calculated for each desorption peak from the desorption profile of Al coated 22MnB5 steel (orange) and Al–Si coated 22MnB5 steel (blue) austenitized at 900 °C during 10 min. (For interpretation of the references to colour in this figure legend, the reader is referred to the Web version of this article.)

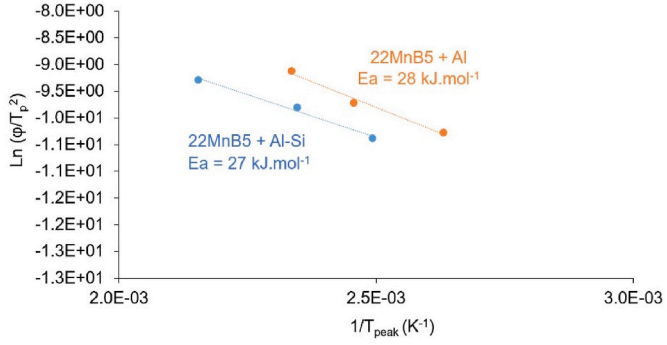

Fig. 10. Choo-Lee plot calculated for each desorption peak from the desorption profile of Al coated 22MnB5 steel (orange) and Al–Si coated 22MnB5 steel (blue) after heat treatment at 900 °C during 10 min after grinding. (For interpretation of the references to colour in this figure legend, the reader is referred to the Web version of this article.)

3.5. Degassing at room temperature

An alternative way to assess the reversibility of trapping of H or D is to perform degassing experiments at room temperature. Indeed, reversible traps can release H or D at low temperature during TDA (below 300 °C) or at room temperature.

Table 3
Detrapping energies (E_d) calculated from Choo-Lee plots (Figs. 9 and 10) obtained for each desorption peaks deconvoluted from desorption profiles of Al and Al–Si coated steel heated treated at 900 °C during 10 min before and after grinding (Figs. 7 and 8).

Sample type	T_{peak} (°C)	R^2	E_d (kJ.mol^{-1})
22MnB5 + Al–Si	159	0.999	27
	210	0.991	35
	400	0.998	77
22MnB5 + Al	147	0.996	32
	250	0.999	53
	500	0.982	140
22MnB5 + Al after grinding	155	0.985	28
22MnB5 + Al–Si after grinding	160	0.989	27

Fig. 11 shows the D_2 desorption profile of Al coated steels after austenitization at 900 °C during 10 min and after 30 days of degassing at 20 °C. All D_2 desorption peaks have strongly decreased in intensity after 30 days of degassing at 20 °C, which means they are related to diffusible D. Fig. 12 presents the evolution of the residual percentage of D calculated for each of these D_2 desorption peaks as a function of the degassing time. A similar decrease can be observed for each desorption peak, pointing out similar detrapping and diffusion processes.

This observation suggests that all the desorption peaks in Al coated steel are related to D located in the same kind of reversible traps. This underlines a contradiction between the nature of D associated with the high temperature desorption peaks in Al coated steel assessed by the degassing method compared to that assessed by the Kissinger theory. Indeed, the activation energies calculated for the D_2 desorption peaks centred at 250 °C and 400 °C are associated with D irreversibly trapped in the sample, while the degassing experiment showed that these desorption peaks are caused by D located in reversible traps. This discrepancy could be explained by different D desorption kinetic behaviours during isothermal holding at 20 °C compared to that during TDA. Previous studies performed isothermal H degassing of Al–Si coated steels at temperature ranging from 25 °C to 250 °C [5,6]. They have shown that the desorption kinetics of H through this material changes at 110 °C. Below this temperature, Al–Si coating prevents H diffusion and H desorbs mainly through the cut edges of the steel substrate. At T > 110 °C, H diffusion occurs mainly through the coating. Therefore, we can imagine a similar D desorption process occurring during non-isothermal heating. As a consequence, during the temperature ramp, D initially desorbs through the bare edges of the steel substrate below 110 °C, then D would start to desorb through the coating, which presents a lower D diffusivity, explaining the emergence of D_2 desorption peaks at higher temperatures. This barrier effect of the coating to H diffusion has already been demonstrated in the literature for the Al–Si coated 22MnB5 steels for the desorption peaks appearing at 200 °C [18,19]. In this work, we confirm that this barrier effect is also observed for Al coated steel, and cause a fraction of diffusible D, initially in the steel

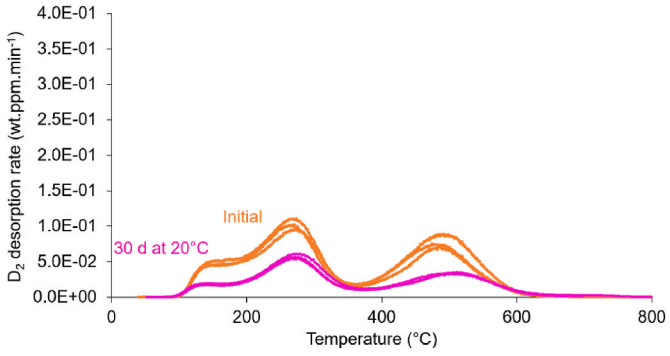

Fig. 11. D_2 desorption curves of Al coated steel after heat treatment and after 30 days of degassing at room temperature.

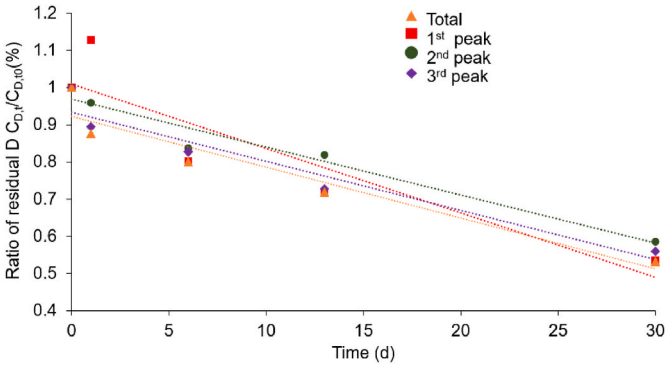

Fig. 12. Evolution with the degassing time at room temperature of the residual concentration of D associated with each desorption peak for Al coated steel. This residual concentration is calculated by taking the ratio of the concentration of D after exposure for t days ($C_{t,D}$) to the concentration of D initially found in the material after austenitization ($C_{t0,D}$).

substrate, to escape through the coating at 500 °C, leading to the third desorption peak at 500 °C.

An interdiffusion layer and Fe_2Al_5 phase are found in both coatings (Fig. 1.1). It has been shown in the literature that Fe_2Al_5 phase presents a lower H diffusion coefficient than martensite, ferrite or FeAl due to its orthorhombic crystal structure, which is a denser packing structure than the BCC crystal structure of the ferrite layer or FeAl layer [32]. Besides, previous work have shown that addition of 3 at % of Al or Si in solid solution in ferrite leads to a decrease of the hydrogen diffusivity by a factor 2 [33–35]. In the case of aluminized steels austenitized at 900 °C during 10 min, the Al and Si contents in the ferrite layer is up to 17 at % and 8 at %, respectively which should further reduce D diffusivity. These authors have attributed this decrease of hydrogen diffusion coefficient to the elastic (mechanical) trapping caused by crystal lattice expansion and chemical trapping of hydrogen nearby the substitute element. As a result, it can be suggested that Fe_2Al_5 and Fe (Al,Si) phases delay D desorption through Al and Al–Si coatings and they are responsible for the shift of desorption peaks at temperatures higher than 200 °C in aluminized steels compared to bare steel.

Fig. 13 shows the D_2 desorption profile of Al–Si coated steels after austenitization at 900 °C during 10 min and after 30 days of degassing at 20 °C. D_2 desorption peaks centred at 150 °C and 200 °C decrease significantly after 30 days of degassing at 20 °C, while the third desorption peak centred at 400 °C, does not decrease as significantly as the first two desorption peaks, even if it is less intense. Fig. 14 shows that the evolution of the residual percentage of D associated to the third desorption peak is slower than the evolution of residual percentage

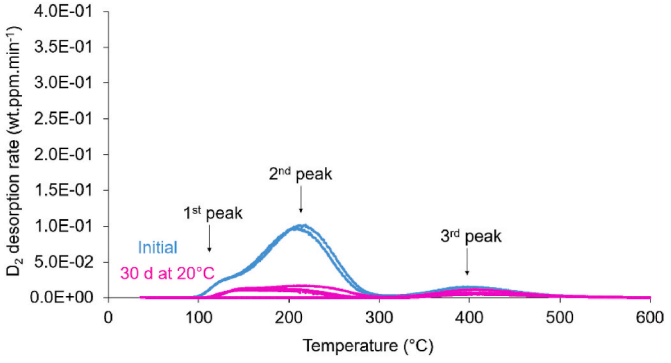

Fig. 13. D_2 desorption curves of Al–Si coated steels as heat treated and after 30 days of degassing at room temperature (pink). (For interpretation of the references to colour in this figure legend, the reader is referred to the Web version of this article.)

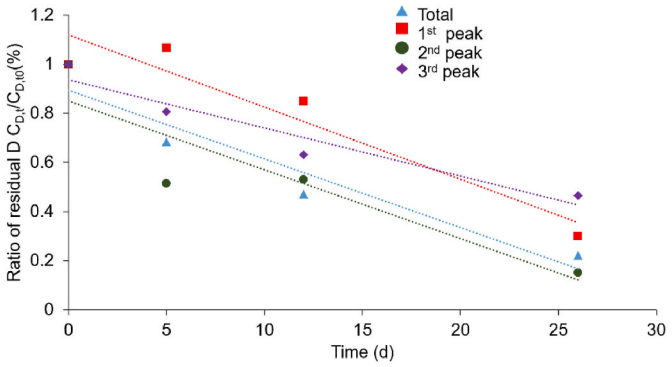

Fig. 14. Evolution with degassing time at room temperature of the residual concentration of D associated with each desorption peak for Al–Si coated steel. This percentage is calculated by taking the ratio of the concentration of D after exposure for t days ($C_{t,D}$) to the concentration of D initially found in the material after austenitization ($(_{t0,D}$).

associated with the first and second ones.

For Al–Si coated steel, the first two desorption peaks thus seem to be related to diffusible D contrary to the third desorption peak, which seems to correspond to D more deeply trapped in the material. This last D_2 desorption peak cannot correspond to D irreversibly trapped in the steel substrate, as the only trap characterized by TDA in coating stripped samples is reversible and presents a low activation energy. The fact that degassing kinetics at room temperature is slower for Al coated steel than Al–Si coated steel could be explained by a lower barrier effect to D diffusion of the Al–Si coating compared to the Al coating.

As a conclusion of this study, the three D_2 desorption peaks in Al coated steel are related to diffusible D located in the dislocation strain field in the steel substrate The presence of D_2 desorption peaks at 250 °C and 500 °C are assigned to slower D diffusion through the coated faces. In the case of Al–Si coated steels, the first two D_2 desorption peaks are related to D trapped in the dislocation strain field in the steel substrate, while the third D_2 desorption peak could be related to D trapped in the coating.

3.6. Effect of aluminized sample size on D_2 desorption profiles

So far, the three D_2 desorption peaks observed on TDA profiles of Al coated steels and the first two desorption peaks in Al–Si coated steels are explained by D trapping in reversible traps in the steel substrate. Their occurrence at different temperatures is due to a barrier effect of the coating to D diffusion and a preferential diffusion by the bare edges at low temperature compared to the coating faces at higher temperature.

In order to confirm this hypothesis, the effect of sample size on thermal desorption profiles of aluminized steels was also investigated. By decreasing the sample size while keeping the same thickness, the proportion of uncoated surfaces (edges) increase and the proportion of coated surfaces decrease. This would promote D desorption from bare edges at the expense of D desorption from coated faces. A set of desorption measurements was thus performed on aluminized samples of different sizes, as illustrated in Figs. 15 and 16. Those Figures show that the size reduction of Al and Al–Si coated samples leads to an increase of the intensity of the first D_2 desorption peak while the intensity of the third D_2 desorption peak decreases.

Figs. 17 and 18 show the evolution of the D concentrations associated to each desorption peak as a function of the uncoated surface ratio, the latter highlighting the importance of uncoated area. Each desorption peak has its own evolution while the total concentration of desorbed D remains constant. The concentration of D associated with the first desorption peak increases with the ratio edge to total surface. This means that a higher proportion of D desorbs from the bare edges of the steel substrate and provides a strong evidence that the first desorption

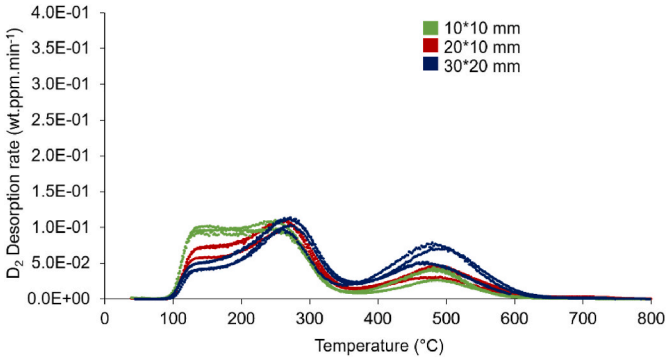

Fig. 15. Evolution of the D_2 desorption profile of Al-coated steels treated at 900 °C for 10 min as a function of sample size, ranging from 10*10 mm to 30*20 mm.

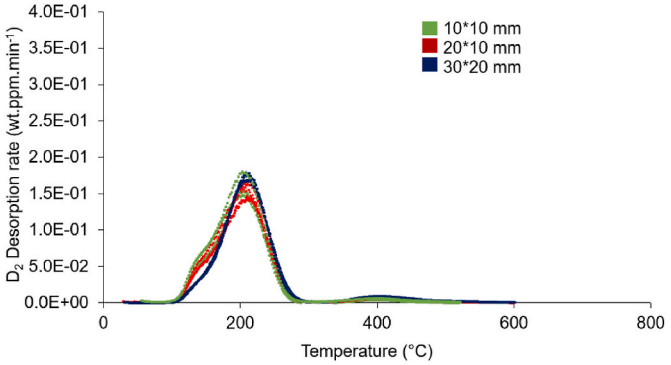

Fig. 16. Evolution of the D_2 desorption profile of Al–Si coated steels treated at 900 °C during 10 min as a function of sample size ranging from 10*10 mm to 30*20 mm.

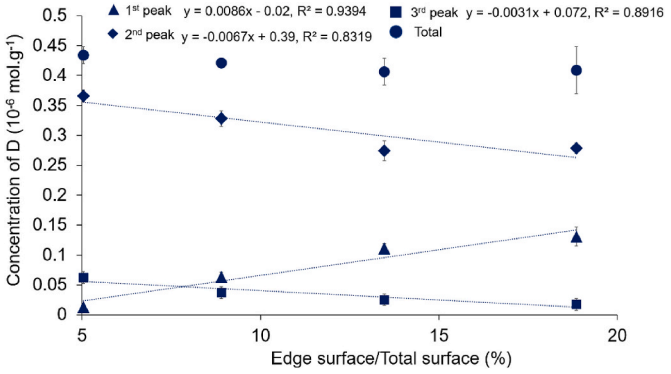

Fig. 17. Evolution of the concentration of D in Al coated steels treated at 900 °C for 10 min, associated with each desorption peaks fitted using gaussian function, as a function of the edge area/total area ratio. This ratio was calculated using the total thickness of Al and Al–Si coated samples after heat treatment (1.25 mm) and the thickness of the coating (approximately 40 μm).

peak in Al–Si and Al coated steels is related to the desorption of D from cut edges of the steel substrate. Furthermore, concentrations of D associated with the second and third desorption peaks decrease along with the reduction of ratio edge to total surface. Indeed, there is more D desorbing through the cut edges for smaller coated specimens at low temperature, which led to a decrease of the remaining D in the steel substrate which can desorb through coated faces. In addition, the first and second desorption peaks in desorption profiles of aluminized steels strongly overlap, which makes their decomposition complicated.

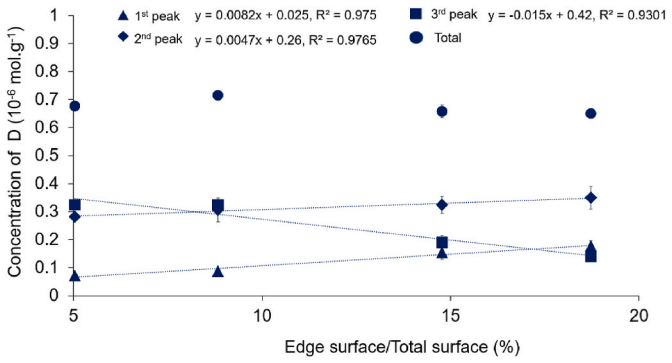

Fig. 18. Evolution of the concentration of D for each desorption peak in Al–Si coated steels treated at 900 °C for 10 min, associated with each desorption peaks fitted using gaussian function, as a function of the edge area/total area ratio. This ratio was calculated using the total thickness of Al and Al–Si coated samples after heat treatment (1.25 mm) and the thickness of the coating (approximately 40 μm).

Therefore, we demonstrate that D is trapped in the steel substrate and gives rise to all desorption peaks on D_2 desorption profiles of aluminized steels. Indeed, the first desorption peak is related to D diffusing through the cut edges. Desorption peaks appearing at higher temperatures are related to D desorbing through the coated faces.

4. Conclusion

Hydrogen trapping in aluminized PHS was critically assessed owing to the use of D and TDA. The main conclusions of this study are as follows:

1) H in aluminized PHS is trapped in the steel substrate and located in the dislocation strain fields which is known to be a reversible trapping site.
2) Multiple peaks on D_2 desorption profiles of Al and Al–Si coated steels are explained by the preferential diffusion path of D depending on the sample temperature. At low temperature, D desorbs from the cut bare edges of the steel substrate, explaining that the first desorption peak is centred at 150 °C. Because of the barrier effect of the coating to D diffusion, D starts to desorb through the coating at temperature higher than 150 °C.
3) In the case of Al and Al–Si coated steel, D_2 desorption peaks appearing at temperature higher than 300 °C is also justified by a barrier effect of the coating. As a result, the desorption kinetic will no longer be limited by D detrapping from the steel substrate but rather by D diffusion through the coating. In general, Kissinger analysis is used to assign the type of H trap in metals and alloys from H_2 desorption peaks. This theory should be used with caution for coated systems, in our case, for aluminized steels.
4) An approach combining the separation of the coating from the steel substrate, the determination of the trapping energy through Kissinger analysis for bare and coated steels as well as a degassing experiment at ambient temperature is advised to critically assess H trapping sites in aluminized PHS.

Perspectives

This paper provides a basis for the correct interpretation of thermal desorption profiles of aluminized steels. The developed methodology is used to assess the diffusible nature of hydrogen and its localization in aluminized steels. However, a number of questions remain unanswered concerning the impact of cracks and the chemistry of the coating on D desorption.

Indeed, these cracks could be associated to area where D desorption will be promoted. Therefore, the D desorption in aluminized steel could occurred in a first step through the ferrite layer and then through Fe_2Al_5. A combination of different crack densities and reduced amount of Al in the ferrite layer in the Al–Si coating compared to Al coated steel could explain why D desorption kinetics at 20 °C during degassing experiment in Al–Si coated steel is faster than in Al coated steel. In order to thoroughly evaluate the impact of cracks on D desorption through the coating, it would be appropriate to vary the density of cracks in the coating before performing TDA or degassing experiments. In this way, the contribution of these cracks to D desorption would be reflected not only in the intensity of desorption peaks, but also on the degassing kinetic.

The effect of the coating's chemistry and microstructure could also be studied by specifically removing each of the coating's phases mechanically and visualize the impact on thermal desorption profiles and the degassing kinetic. These issues will be investigated in a future paper.

Declaration of competing interest

The authors declare that they have no known competing financial interests or personal relationships that could have appeared to influence the work reported in this paper.

Acknowledgements

M. Krid acknowledges the support of the FRIA, Belgium.

References

[1] Taylor T, Clough A. Critical review of automotive hot-stamped sheet steel from an industrial perspective. Mater Sci Technol 2018;7(34):809–61. https://doi.org/10.1080/02670836.2018.1425239.
[2] Bruschi S, Ghiotti A. Hot stamping. Comprehensive Mater Process 2014;3:27–54. https://doi.org/10.1016/B978-0-08-096532-1.00303-4.
[3] Karbasian H, Tekaya AE. A review on hot stamping. J Mater Process Technol 2010;210:2103–18. https://doi.org/10.1016/j.jmatprotec.2010.07.019.
[4] Naderi M. Hot stamping of ultra high strength steels. In: Doctoral thesis. RWTH Aachen University. Germany; 2007.
[5] Georges C, Sturel T, Drillet P, Mataigne JM. Absorption-desorption of diffusible hydrogen in aluminized boron steel. ISIJ Int 2013;53:1295–304. https://doi.org/10.2355/isijinternational.53.1295.
[6] Georges C, Machedo T, Drillet P. Measurements and modelling of hydrogen desorption at room temperature in Al-Si-coated boron steel. In: Proceedings of steel hydrogen conference. Belgium: Gent; 2011. p. 77–88.
[7] Forcey KS, Ross DK, Simpson JCB, Evans DS. Hydrogen transport and solubility in 316L and 1.4914 steels for fusion reactor applications. J Nuclear Mater 1988;160:117–24. https://doi.org/10.1016/0022-3115(88)90038-4.
[8] Forcey KS, Ross DK, Wu CH. The formation of hydrogen permeation barriers on steels by aluminising. J Nuclear Mater 1991;182:36–51. https://doi.org/10.1016/0022-3115(91)90413-2.
[9] Ishikawa T, McLellan RB. The diffusivity of hydrogen in aluminium. Acta Metall 1986;34:1091–5. https://doi.org/10.1016/0001-6160(86)90219-1.
[10] Prakash U, Parvathavarthini N, Dayal RK. Effect of composition on hydrogen permeation in Fe-Al alloys. Intermetallics 2007;15:17–9. https://doi.org/10.1016/j.intermet.2006.02.002.
[11] Kupka M, Stepień K. Hydrogen permeation in Fe-40 at. % Al alloy at different temperatures. Corrosion Sci 2009;51:699–702. https://doi.org/10.1016/j.corsci.2008.11.026.
[12] Young GA, Scully JR. The diffusion and trapping of hydrogen in high purity aluminium. Acta Mater 1998;46(18):6337–49. https://doi.org/10.1016/S1359-6454(98)00333-4.
[13] Pressouyre GMA. Classification of hydrogen traps in steel. Metall Trans A 1979;10:1571–3. https://doi.org/10.1007/BF02812023.
[14] Papavinasam S. Corrosion control in the oil and gas industry. Gulf Professional Publishing. Elsevier; 2014. p. 294–300. https://doi.org/10.1016/B978-0-12-397022-0.00005-4 [Chapter 5], Mechanisms.
[15] Fu ZH, Yang BJ, Shan ML, Li T, Zhu ZY, Ma CP, Zhang X, Gou GQ, Wang ZR, Gao W. Hydrogen embrittlement behavior of SUS301L-MT stainless steel laser-arc hybrid welded joint localized zones. Corrosion Sci 2020;164:108337. https://doi.org/10.1016/J.CORSCI.2019.108337.
[16] Venezuela J, Zhou Q, Liu Q, Li H, Zhang M, Dargusch MS, Atrens A. The influence of microstructure on the hydrogen embrittlement susceptibility of martensitic advanced high strength steels. Mater Today Commun 2018;17:1–14. https://doi.org/10.1016/J.MTCOMM.2018.07.011.
[17] Lynch S. Hydrogen embrittlement phenomena and mechanisms. Corrosion Rev 2012;30(3):105–23. https://doi.org/10.1515/CORRREV-2012-0502/MACHINEREADABLECITATION/RIS.

[18] Pérez Escobar D, Verbeken K, Duprez L, Verhaege M. Evaluation of hydrogen trapping in high strength steels by thermal desorption spectroscopy. Mater Sci Eng, A 2012;551:50–8. https://doi.org/10.1016/J.MSEA.2012.04.078.
[19] Cho L, Sulistiyo DH, Seo EJ, Jo KR, Kim SW, Oh JK, Cho Y, De Cooman BC. Hydrogen absorption and embrittlement of ultra-high strength aluminized press hardening steel. Mater Sci Eng, A 2018;734:416–26. https://doi.org/10.1016/j.msea.2018.08.003.
[20] Jo KR, Cho L, Sulistiyo DH, Seo EJ, Kim SW, De Cooman BC. Effects of Al-Si coating and Zn coating on the hydrogen uptake and embrittlement of ultra-high strength press-hardened steel. Surf Coating Technol 2019;374:1108–19. https://doi.org/10.1016/j.surfcoat.2019.06.047.
[21] Kuhlmann M, Schwedler O, Holtschke N, Jüttner S. Consideration of hydrogen transport in press-hardened 22MnB5. Mater Test 2015;57(11):977–84. https://doi.org/10.3139/120.110808. 12.
[22] Kuhlmann M, Mitzschke N, Jüttner S. Determination of hydrogen transport behaviour in boron-manganese steels using different methods and boundary conditions. Metals 2019;9(9):1007. https://doi.org/10.3390/met9091007.
[23] Mandy M, Georges C, Sturel T, Drillet P, Jacques PJ. On the analysis of the simultaneous uptake and desorption of different isotopes of gaseous hydrogen by advanced high strength steels. Scripta Mater 2019;161:84–7. https://doi.org/10.1016/J.SCRIPTAMAT.2018.09.034.
[24] Windmann M, Röttger A, Theisen W. Formation of intermetallic phases in Al-coated hot-stamped 22MnB5 sheets in terms of coating thickness and Si content. Surf Coating Technol 2014;246:17–25. https://doi.org/10.1016/j.surfcoat.2014.02.056.
[25] Grigorieva R. Etude des transformations de phases dans le revêtement Al-Si lors d'un recuit d'austénitisation. Nancy; 2010.
[26] Windmann M, Röttger A, Hahn I, Theisen W. Mechanical properties of AlXFeY intermetallics in Al-base coatings on steel 22MnB5 and resulting wear mechanisms at press-hardening tool steel surfaces. Surf Coating Technol 2017;321:321–7. https://doi.org/10.1016/j.surfcoat.2017.04.075.
[27] Barreau M, Méthivier C, Sturel T, Allely C, Drillet P, Cremel S, Grigorieva R, et al. In situ surface imaging: high temperature environmental SEM study of the surface changes during heat treatment of an Al-Si coated boron steel. Mater Char 2020;163(1):110266. https://doi.org/10.1016/j.matchar.2020.110266. 12.
[28] Kucera V, Cabibbo M, Prusa F, Fojt J, Petr-Soini J, Pilvousek T, Kolarikova M, et al. Phase composition of Al-Si coating from the initial state to the hot-stamped condition. Materials 2021;14(5):1125. https://doi.org/10.3390/MA14051125.
[29] Cho L, Golem L, Seo EJ, Bhattacharya D, Speer JG, Findley KO. Characteristics and mechanical properties of the Al–Si coating on press hardened 22MnB5 steel. J Alloys Compd 2020;846:156349. https://doi.org/10.1016/j.jallcom.2020.156349.
[30] Choo WY, Lee JY. Thermal analysis of trapped hydrogen in pure iron. Metall Trans A 1982;13(1):135–40. https://doi.org/10.1007/BF02642424.
[31] Blaine RL, Kissinger HE. Homer kissinger and the kissinger equation. Thermochim Acta 2012;540:1–6. https://doi.org/10.1016/j.tca.2012.04.008.
[32] He Y, Li Y, Chen C, Yu H. Diffusion coefficient of hydrogen interstitial atom in α-Fe, γ-Fe and ε-Fe crystals by first-principle calculations. Int J Hydrogen Energy 2017;42(44):27438–45. https://doi.org/10.1016/J.IJHYDENE.2017.08.212.
[33] Hagi H. Diffusion coefficient of hydrogen in iron without trapping by dislocations and impurities. Mater Trans, JIM 1994;35(2):112–7. https://doi.org/10.2320/MATERTRANS1989.35.112.
[34] Sawada H, Omura T. Interaction between hydrogen and solute atoms in bcc iron. Comput Mater Sci 2021;198:110652. https://doi.org/10.1016/J.COMMATSCI.2021.110652.
[35] Tomohiko O, Hideaki S, Kenji K, Yuji A. Effects of alloying elements on hydrogen diffusion in iron. ISIJ Int 2021;61(4):1287–93. https://doi.org/10.1016/J.COMMATSCI.2021.110652.